Surface transport kinetics in low-temperature silicon deposition determined from topography evolution

K. R. Bray and G. N. Parsons
Department of Chemical Engineering, NC State University, Raleigh, North Carolina 27695-7905
(Received 20 October 2000; revised manuscript received 5 June 2001; published 19 December 2001)

In this article, surface transport kinetics during low-temperature silicon thin film deposition are characterized using time dependent surface topography and dynamic scaling models. Analysis of surface morphology indicates that diffusion of adsorbed species dominates surface transport, with a characteristic diffusion length that increases with surface temperature. A diffusion activation barrier of ~ 0.2 eV is obtained, consistent with hydrogen-mediated adspecies diffusion on the growth silicon surface. Samples are compared over a range of deposition temperatures (25 to 350 °C) and film thickness (20 to 5000 Å) deposited using silane with helium or argon dilution, on glass and silicon substrates. Self-similar surface structure is found to depend on detailed film growth conditions, but is independent of film thickness after nuclei coalescence. For films deposited using helium dilution, static and dynamic scaling parameters are consistent with self-similar fractal geometry scaling, and the lateral correlation length increases from 45 to 150 nm as temperature increases from 25 to 150 °C. These results are discussed in relation to current silicon deposition models and with topography evolution observed during low temperature growth of other amorphous material systems.

DOI: 10.1103/PhysRevB.65.035311 PACS number(s): 68.43.Jk, 68.55.Jk, 81.15.Gh

I. INTRODUCTION

A current challenge in low temperature thin film deposition is to understand kinetics of surface processes to control surface reactions and improve material properties. Growth models based on thermodynamic balances only strictly apply in the equilibrium limit, where mass transport on the surface is fast relative to the arrival of depositing species. This limit is impractical for current technologically relevant processes where high deposition rates, smooth surfaces, limited disruption of substrate materials (i.e., dopant profiles, polymer structure, bond structure, and composition, etc.), and controlled reactivity at the surface are critically important. The technological need for lower deposition temperatures requires that the deposition procedure be maintained far from equilibrium, where kinetic rate processes dominate surface mechanisms. Therefore, understanding thermally activated elementary process steps is particularly important to describe film growth, and kinetic processes have received significant attention theoretically and experimentally over the past several years.[1–6]

Hydrogenated amorphous silicon (*a*-Si:H) can be deposited by a variety of low temperature techniques, including plasma enhanced chemical vapor deposition, reactive sputtering, and hot wire chemical vapor deposition. Mechanisms in *a*-Si:H deposition continue to receive attention because of the push to improve material defect density and stability for commercial applications, including solar cells and thin film transistor devices. Also, hydrogenated amorphous silicon is a good model system to understand activated low temperature deposition processes because the process proceeds from a single precursor (silane) in commonly available direct rf plasma deposition tools.

Plasma deposition of hydrogenated amorphous silicon results in very smooth, conformal surfaces and nonthermally activated growth rates over temperatures ranging from <25 to 400 °C. Typical models for *a*-Si:H growth presume that radical precursors generated in the gas phase adsorb and diffuse on the surface with low thermal barriers, giving rise to the observed smooth conformal surface coverage.[4–6] Surface transport parameters are typically characterized by comparing experimental macroscopic parameters (such as growth rate or step coverage) with precursor dependent reaction models,[7,8] or are estimated through simulations.[4,6,9–11] To date, results directly identifying surface transport kinetic processes in low temperature silicon growth are not available. The technique for surface transport analysis presented and utilized here employs direct surface characterization, and does not require identification or supposition of the particular gas-phase precursor responsible for growth, or the adsorbed surface species responsible for diffusion.

Results presented below demonstrate that silicon surface transport during low temperature plasma deposition is dominated by thermally activated adspecies diffusion, with an activation barrier of 0.2 eV. The diffusion barrier is an important parameter for kinetic growth models for silicon, and this work presents a unique direct experimental characterization of this parameter. The basic approach used here has been used previously to characterize surface diffusion during physical vapor deposition of glassy metals.[12] This article addresses limitations and requirements for applying this method to analysis of silicon deposition, and demonstrates differences between deposition of hydrogenated silicon and other materials.

II. DYNAMIC SCALING, AND DEFINITION OF SURFACE SCALING PARAMETERS

A. Characterization of surface morphology

Surface morphology of deposited films, determined using scanning electron microscopy, scanning probe microscopy, or small angle x-ray scattering techniques, is typically analyzed using a height-height correlation function

 ©2001 The American Physical Society

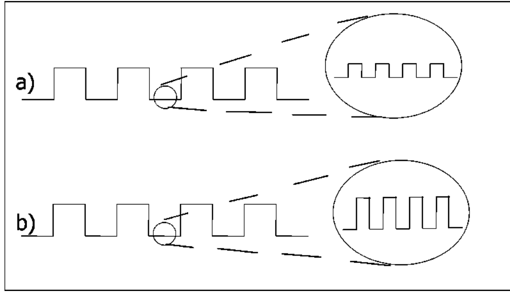

FIG. 1. Artificial self-similar and self-affine profiles. Isotropic magnification of (a) self-similar and (b) self-affine profiles are shown in the circles.

$$C(R)=\langle z(r)z(r+R)\rangle_{r,R} \quad (1)$$

or a height-difference correlation function

$$G(R)=\langle [z(r)-z(r+R)]^2\rangle_{r,R}, \quad (2)$$

where $z(r)$ is the height at any point r on the surface and $\langle\rangle_{r,R}$ refers to the average over all pairs of surface points separated by a distance R. The data is then compressed and displayed in terms of a power spectral density function

$$g(|\mathbf{q}|)=F[C(|\mathbf{r}|)], \quad (3)$$

where F is the two-dimensional Fourier transform operator. Early models used Gaussian or modified Gaussian functions to describe and predict surface correlation functions,[3] which allowed the surface structure to be described by a minimal set of parameters including the standard deviation of the surface height, and the lateral correlation length. Later models utilized concepts of topographical scaling, where surface self-affinity or surface self-similarity is used to describe growing surfaces.[1] A surface that follows fractal growth is self-affine, indicating a correlation between roughness amplitude and lateral scale. Self-similarity is a special case of self-affinity, where the roughness exhibits isotropic scaling[2] with a constant ratio between the vertical and lateral components, independent of lateral scale. The distinction between self-affinity and self-similarity is shown schematically in Fig. 1. The height-difference correlation function can also be written in terms of a scaling function $f(R/L_c)$:

$$G(R)=2\sigma^2 f(R/L_c), \quad (4)$$

where σ is the root mean square (rms) roughness of the surface and L_c is the maximum lateral length scale over which surface roughness correlations persist.[3] The scaling function has an asymptotic form $f(x)=(R/L_c)^{2\alpha}$ for $x<1$, and $f(x)=1$ for $x>1$, where α is the static scaling coefficient (or Hurst parameter). Values for the static scaling coefficient range from 0–1, with α approaching 0 for jagged surfaces and 1 for smooth surfaces.[13] For the dynamic scaling hypothesis proposed by Sinha *et al.*,[14] the height-height correlation function is written as an exponential

$$C(R)=\sigma^2\exp[-(R/L_c)^{2\alpha}]. \quad (5)$$

Dynamic scaling also predicts that for a self-affine surface, the root-mean-square roughness of the surface scales as

$$\sigma\sim R^\alpha f(t^\beta/R^\alpha), \quad (6)$$

where t is the deposition time (proportional to film thickness) and β is the dynamic or temporal scaling exponent.[3,15] When the argument of function f is much less than 1, then f approaches t^β/R^α and when the argument is greater than 1, f is constant. This indicates that the rms roughness will be a function of the length scale (R) used for the analysis until the roughness value saturates at a constant value (σ_{sat}) for large lengths. For a self-affine surface, a log-log plot of σ vs R will yield a straight line with slope between 0 and 1 for $R<L_c$. For the more restricted case of a self-similar surface, the same functional form holds with $\alpha=1$.

The Fourier transform of the dynamic scaling autocorrelation function results in the spectral density function $g(|\mathbf{q}|)=[\alpha\sigma^2L_c^2/\pi]$ for $|\mathbf{q}|<1/L_c$, and $g(|\mathbf{q}|)=[\alpha\sigma^2/L_c^{2\alpha}\pi]q^{-2(\alpha+1)}$ for $|\mathbf{q}|>1/L_c$. The quantity $i=2(\alpha+1)$ is the Fourier index, and will have a value between 0 and 4 for a self-affine surface, and will be ~ 4 when the surface is self-similar. For growth on a two-dimensional surface, the static scaling exponent and the Fourier index are related through the fractal dimension,[3,16] $D_f=(8-i)/2$, which is also related to α by $D_f=(3-\alpha)$.

Surface kinetic models describe the balance between random arrival of species from the gas phase and a variety of thermally activated processes that operate on the surface. For growth of thin films from the vapor phase, if the species responsible for film deposition are randomly incorporated into the surface without appreciable surface transport, then stochastic, or random, surface growth will result in a rough surface. In the early 1950's, Herring described four distinct surface transport mechanisms that reduce surface roughness: (i) viscous flow, (ii) evaporation-condensation, (iii) bulk diffusion, and (iv) surface diffusion.[17] The relationship between the surface topography and the surface transport mechanism comes from an analysis of the time and amount of material needed to produce a geometrically similar change in two different sized clusters using each mechanism. These mechanisms leave distinct imprints on the topography that are recognizable through fractal analyses. In 1986, Kardar, Parisi, and Zhang described the development of surface roughness based on symmetry arguments.[18] Later models related the symmetry models to transport processes using equations of motion with terms corresponding to specific surface smoothening or roughening mechanisms.[3] Continuum models including linear and nonlinear terms in the equations of motion are used to analyze surface roughness data to determine scaling coefficients under different conditions. Matching the experimentally determined scaling exponents with continuum growth models then identifies the primary transport mechanisms.

B. Determination of scaling parameters

Both the static scaling coefficient α and the dynamic scaling coefficient β are needed to distinguish surface transport

mechanisms uniquely. Two methods, dimensional and frequency analysis are used to analyze topography data. Dimensional analysis involves determining rms surface roughness at various length scales (L) and deposition times (t), then obtaining scaling coefficients[3,19] using $\sigma \sim L^{\alpha}$ and $\sigma_{\mathrm{sat}} \sim t^{\beta}$. Frequency analysis utilizes the Fourier transform of the surface topography[16,20] to obtain the power spectral density (PSD). The one-dimensional PSD is obtained by using the radius in reciprocal space as the spatial frequency and radially averaging the two-dimensional spectrum.[21] The Fourier index is determined from the PSD using the power law relationship PSD $\sim q^{-i}$ for wave numbers q greater than a critical frequency q_c (inverse of the critical length $q_c = 1/L_c$), and α is determined directly from i. Radial averaging generally gives a better correlation with fractal dimension than linear averaging.

For the linear continuum model with surface transport dominated by surface diffusion, the scaling coefficients are expected to attain values of $\alpha = 1$ and $\beta = 0.25$.[2,3,22] When nonlinear terms are included, scaling coefficients of $\alpha = 0.67$ and $\beta = 0.2$ are expected for diffusion.[2] For transport by evaporation and condensation,[3] expected values are $\alpha = 0$ and $\beta = 0$. There are several reports analyzing kinetic smoothening mechanisms of hydrogenated amorphous silicon deposited using plasma deposition[23,24] and thermal evaporation.[25] Typically, α is measured between 0.8–1 and β between 0.2–0.33, consistent with self-similar geometry and transport by surface diffusion. As expected, these values are distinctly different from parameters typically reported for evaporated metal surfaces. Static scaling coefficients are typically $\sim$0.7–0.8 with $\alpha = 0.82$ for Ag and $\alpha = 0.68$ for Pt,[22] which are consistent with values reported for surface diffusion and step growth,[3,22] i.e., $\alpha = 0.67$ and $\beta = 0.2$.

III. EXPERIMENTAL METHOD

A. Hydrogenated amorphous silicon deposition

To analyze silicon deposition processes, films were deposited using an rf (13.56 MHz) parallel plate plasma deposition system with circular geometry (diameter=28 cm) and radial gas flow. Deposition temperature ranged from 25 to 150 °C, and film thickness was varied from 20 to 5000 Å. Film thickness was determined by step-height profilometry for films >100 Å, and from the extrapolated growth rate for thinner films. Growth rate was linear for all conditions. Silane gas, diluted to 2% with He and/or Ar, was used for the depositions, and the total gas flow rate was fixed at 100 standard cubic centimeters per minute (sccm). The process pressure was fixed at 0.6 Torr, and the rf power was 8 mW/cm^2. Using SiH_4/He gas mixtures, the deposition rate was $\sim$50 Å/min, and slower rates ($\sim$22 Å/min) were observed using SiH_4/Ar mixtures. Substrates included clean Si(100) and 7059 glass.

B. Topography analysis

Atomic force microscopy (AFM) for surface topography analysis was conducted using a Digital Instruments Dimension 3000, with a Nanoscope IIIa controller and vibration-shielded hood. Imaging was performed in intermittent contact mode, using c-Si cantilever probes with a nominal tip radius of $5-10$ nm. Image analysis was performed using built-in software functions to calculate the root-mean-square roughness σ and the power spectral density (PSD) spectrum. The rms roughness is computed using the function

$$\sigma = [\Sigma (Z_i - Z_{\mathrm{ave}})^2 / N]^{1/2}, \tag{7}$$

where Z_{ave} is the average height in a given area, Z_i is the height of a given point, and N is the number of points in the area. The PSD is calculated from an algorithm that is based on radially averaging the two-dimensional fast Fourier transform of the image. Scan sizes of 200×200 nm^2, 500×500 nm^2, and 1×1 μm^2 were measured to insure there were no artificial effects introduced into the analysis from the scan size. The probe tip was changed as needed to maintain good images.

All AFM measurements were performed under ambient conditions. An important consideration is the effect of probe tip size and geometry, and surface ambient exposure, on surface topography results. To address this question, a 480 nm thick a-Si film deposited at 350 °C and previously characterized using STM directly connected to a plasma deposition reactor[26] was analyzed in ambient in our lab using AFM. Using the same range of scan sizes (50 to 250 nm), the radially averaged Fourier transform of the on-line STM measurement showed a slope of $\sim$1.2, and the AFM measurement produced a slope of 1.2–1.3, indicating that ambient exposure does not significantly affect surface topography over the height and length scales analyzed. The AFM analysis was able to extend to scan sizes greater than 1 μm which enabled a greater range of frequencies for analyzing the power spectrum. The AFM will generally have a larger tip radius than the STM, which will allow the STM to better access topography data over short (<10 nm) length scales. However, for the dimensional analysis, the smallest roughness calculations performed used length scales exceeding 20 nm, which is larger than twice the nominal AFM tip radius. Therefore, for the length scales of interest, ambient AFM and on-line STM techniques give reasonably similar results, and the AFM images are sufficient to extract useful topography data and surface scaling parameters.

IV. RESULTS AND DISCUSSION

A. Frequency and dimensional analysis to characterize fractal scaling

Extraction of surface scaling parameters from the fractal dimension requires that the surface structure follow fractal geometry scaling. Therefore, we first demonstrate that self-similar surface scaling can be achieved over a wide range of process conditions (but not all conditions) for a-Si:H deposition. Also, for demonstration and experiment control, the amorphous silicon surface is compared to an evaporated aluminum surface, which is expected to exhibit substantially different surface topography and scaling. Topography is analyzed using both frequency and dimensional analysis.

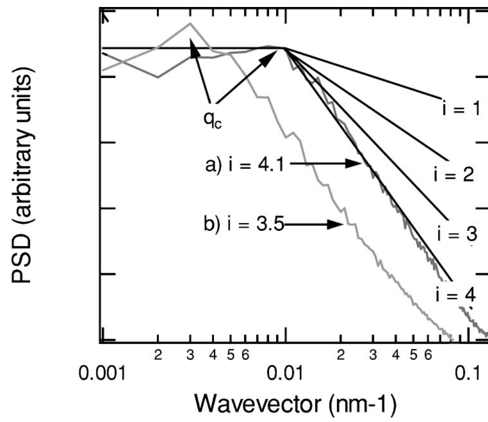

FIG. 2. Power spectral density plots for (a) 1000 Å a-Si:H film deposited by plasma CVD from SiH_4/He and (b) 1.5μm Al deposited by evaporation. The spectrum is observed to decrease with a slope of i, the Fourier index, above the critical frequency q_c. The a-Si has a larger value for i, indicating surface diffusion is more prominent than in the evaporation process.

Figure 2 shows the power spectral density used for frequency analysis for two samples: sample (a) is a 1000 Å a-Si:H deposited using a silane plasma diluted with helium and sample (b) is a 1.5 μm thick evaporated aluminum film. For both surfaces, the PSD has an almost constant value in the low frequency range. This relates to large real space features and a substantial change in roughness is not expected on that scale. Above the critical frequency ($q_c = 0.01$ nm^{-1} for Si and 0.003 nm^{-1} for Al in the spectra shown), the PSD decreases exponentially on the log-log plot with a $1/q^i$ dependence with $i = 4.1$ for a-Si and $i = 3.5$ for the Al surface.

For dimensional analysis, the static scaling exponent is determined for the same Si and Al surfaces from the plot shown in Fig. 3(a). The plot of rms surface roughness vs measurement length gives a linear slope of α up to the critical length,[3,22] L_c and the roughness saturates at σ_{sat} for large lengths. The a-Si film shows a value of $\alpha = 1.03$, consistent with self-similar scaling, and the Al film has a value of $\alpha = 0.77$, which is in the expected range for evaporated metals.[22] The data in Fig. 3(a) indicate critical lengths for these a-Si and Al samples are $L_c = 75$ and 330 nm, respectively.

Generally for silicon films deposited using SiH_4/He mixtures, including the films shown in Figs. 2 and 3, dimensional analyses result in values that saturate at $\alpha \approx 1$, and frequency analyses result in Fourier index $i \approx 4$. These values are both consistent with self-similar scaling geometry in the surface morphology of deposited silicon films. As will be shown below, deposition using argon dilution disrupts the self-similar scaling geometry.

B. Effect of thickness and gas composition on scaling coefficients

The surface topography was examined for silicon plasma deposition as a function of temperature, film thickness, and diluent gas species. Specifically, static scaling coefficient values were extracted using dimensional analysis for silicon deposited from SiH_4/He and SiH_4/Ar mixtures on crystalline silicon substrates for various deposition times. The static scaling coefficient was observed to increase during the initial growth (corresponding to film nucleation and coalescence, as shown below), then saturate at $\alpha = 1.09 \pm 0.05$ for He dilution and $\alpha = 0.63 \pm 0.01$ for Ar dilution. The smaller saturation value for Ar diluted silane indicates a distinctly different (non-self-similar) surface topography for the Ar diluted process. This difference in surface topography between Ar and He dilution is presumably due to the larger energy transfer during Ar ion bombardment. For comparison, Fourier index values are determined from frequency analysis for a-Si:H films deposited from SiH_4/He. The values for i are constant with $i = 4.1 \pm 0.3$ for deposition times from 1 to over 30 min, corresponding to thicknesses greater than 1500 Å. Using the relationship between α and i, the Fourier index obtained from frequency analysis corresponds to $\alpha = 1.05$, which is consistent with α obtained using dimensional analysis on the same set of films. This result further supports the self-similar structure of the growing a-Si:H surface. Thicker films have also been measured and indicate that self-similar behavior extends to film thickness at least as large as 5000 Å.

For films grown with helium dilution at 25 and 100 °C, the dynamic scaling exponent, β, is determined from the slope of σ_{sat} plotted vs deposition time shown in Fig. 4. For short deposition times, the surface roughness values are not expected to follow the scaling trend because the silicon nuclei have not completely coalesced. A least squares fit to the points for deposition $\geqslant 1$ min results in $\beta = 0.26 \pm 0.13$. For this self-affine surface, the coefficients of $i \approx 4$, $\alpha \approx 1$, and $\beta \approx 0.25$ are consistent with surface transport dominated by adatom diffusion.[2,3,22] Further support for surface diffusion is obtained from analysis of nuclei coalescence in the initial stages of film growth.

C. Silicon nucleation and film coalescence

Film coalescence can be directly observed using AFM analysis and related to observed trends in the static scaling coefficient. Figure 5 shows AFM images for films deposited for 30 sec at (a) 25 and (b) 100 °C. The nuclei in the 25 °C film are small (17 nm) and jagged, whereas the 100 °C film exhibits larger (45 nm), rounder nuclei. Note that the vertical scale for sample (b) is 10× larger than sample (a). The static scaling coefficient for the image in Fig. 5(a) is ~0.25, similar to that measured for the clean substrate. The film deposited at 100 °C in Fig. 5(b) has $\alpha = 0.8$, close to $\alpha \approx 1$ observed for thicker films. The AFM images and roughness analysis indicate the nuclei are not yet coalesced at low temperature, but they have begun to coalesce at higher temperature. At longer deposition times, AFM images in Fig. 6 indicate complete coalescence, and films show surface morphology independent of substrate temperature, consistent with the constant scaling coefficient observed.

Figure 3(b) shows the rms roughness vs length scale for a-Si films deposited from SiH_4/He mixtures on silicon substrates, for deposition times ranging from 10 to ~1200 s. The slope of the curves α are small for short deposition time

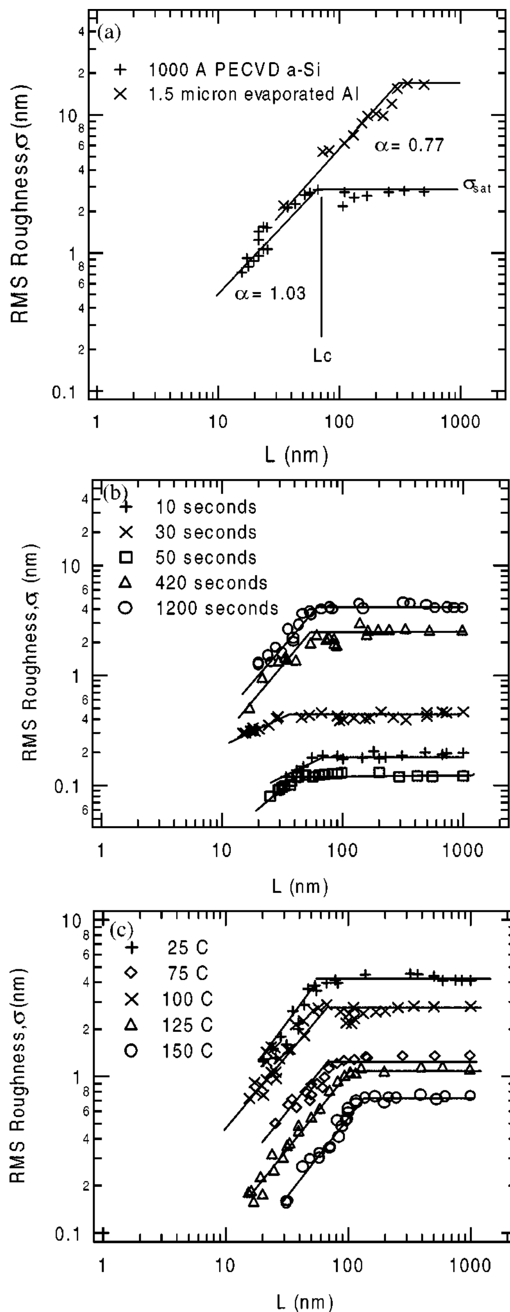

FIG. 3. rms roughness vs length scale. (a) Comparison between PECVD a-Si:H and evaporated Al. Evaporated Al has a smaller α, indicating it has a rougher surface than the plasma deposited a-Si. The roughness of the a-Si film saturates at a critical length L_c of 75 nm. (b) Comparison of deposition time for films deposited at 25 °C. The static scaling coefficient α, remains small for thin (noncoalesced) films, and then reaches a constant value for thick films. (c) Comparison of substrate temperature for films deposited from a SiH_4/He mixture for 20 min.

(similar to values measured for the clean silicon substrate) and increase and saturate for longer times. Values for α determined from data in Fig. 3(b) and from other films deposited at various temperatures on silicon and glass substrates are plotted versus deposition time in Fig. 7. The value for α increases with deposition time then saturates near $\alpha = 1$. The transition from the initial α value to the saturated value corresponds to nuclei coalescence observed in the AFM images, and the horizontal arrows in Fig. 7(a) indicate the range of coalescence times determined from AFM. The time required to reach saturation decreases with increasing temperature, indicating that films coalesce more rapidly at higher temperature, consistent with thermally activated surface diffusion. A plot of the inverse inflection time vs $1/T$ gives an activation energy of ~ 0.07 eV for films deposited on silicon. The data in Fig. 7(b) shows that nucleation and coalescence occurs at a slower rate on glass than on clean silicon substrates. A summary of scaling parameters (from dimensional and frequency analysis), coalescence times, and correlation lengths, obtained from silicon films deposited using various source gases, substrates, and substrate temperatures is given in Table I.

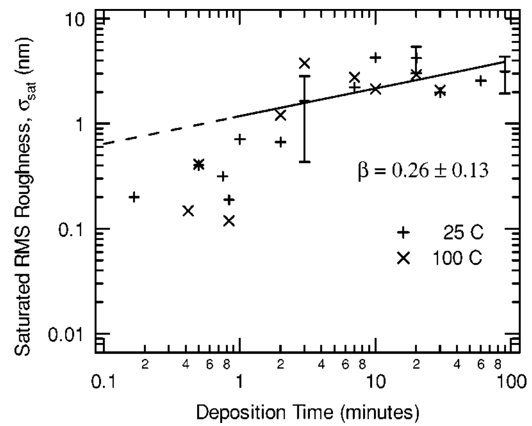

FIG. 4. Saturated rms roughness (determined by dimensional analysis) vs deposition time for silicon deposited from SiH_4/He mixtures on Si. The surface diffusion model indicates that σ should increase with time with a slope of $\beta = 0.25$. At times greater than one minute, a best fit of the roughness data yields $\beta = 0.26 \pm 13$. The error was determined from the quality of the least squares fit. The dashed line is an extension of the fit and does not represent a fit of the data in that region of the graph. The error bars are 3σ values determined from >5 measurements of multiple films deposited with the same conditions.

D. Effect of temperature on surface transport during silicon deposition

Figure 3(c) shows the rms roughness vs length scale for 1000 Å thick a-Si:H films deposited from silane/helium mixtures at various temperatures. Over the range studied, the slope $\alpha = 1.09 \pm 0.05$ and is independent of temperature. However, as temperature increases, the saturation roughness decreases, and the correlation length L_c is observed to increase. The correlation length is a good estimate of the surface diffusion length[4,23] and has been used to evaluate activation barriers for surface diffusion for glassy metals formed by physical vapor deposition.[12] The surface diffusion coefficient is proportional to the square of the diffusion length. Figure 8 shows an Arrhenius plot of $\ln(L_c^2)$, determined from the data in Fig. 3(c). The data shows a good fit to a straight line and the slope indicates an activation energy of E_a

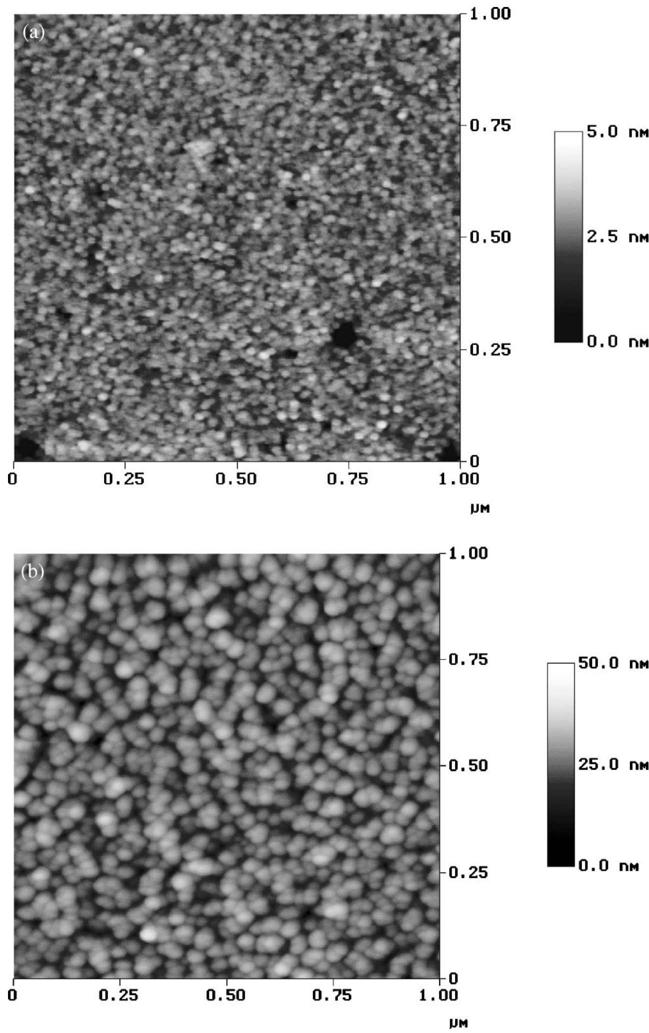

FIG. 5. Initial nucleation of a-Si films grown for 30 s at (a) 25 °C and (b) 100 °C. The films have coalesced. The 25 °C film has small, jagged nuclei, while the 100 °C film has larger, rounder nuclei.

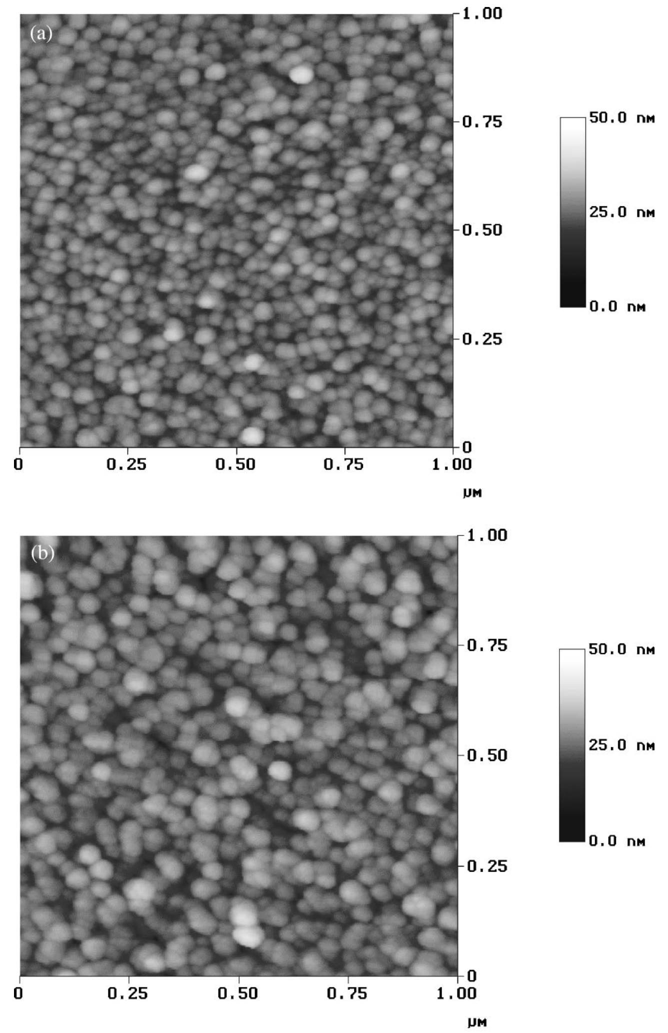

FIG. 6. Fully developed nucleation of films grown for 3 min at (a) 25 °C and (b) 100 °C. There are no distinguishable differences between the topographies of the surfaces.

$=0.20\pm0.02$ eV. Therefore, the data in Figs. 3, 4, 7, and 8 are consistent with surface transport in a-Si:H deposition being dominated by adspecies diffusion with an activation barrier of 0.2 eV. Other indirect estimates of surface diffusion activation barriers during a-Si:H growth[4,6,7,9–11] are typically in the range of 0.16 to 0.3 eV. The value we obtain is within this range, but it is important to note that the approach used here involves direct evaluation of deposited surfaces using a model of surface topography evolution not previously used to characterize surface transport kinetics in silicon growth.

Surface diffusion barriers determined from analysis of glassy metal surfaces formed by physical vapor deposition are significantly larger than that found here for silicon deposition. The smaller barrier in our analysis is consistent with a hydrogen-mediated precursor diffusion process. Diffusion on a clean glassy metal surface requires direct metallic bond breaking and reforming, so a barrier close to the bond enthalpy is expected. For hydrogenated silicon growth, barriers less than the bond enthalpy are expected due to the reduction of surface energy by bonded surface hydrogen. Silyl precursor adsorption on hydrogenated silicon surfaces is typically believed[4–6] to involve formation of a surface three-center bond (Si-H-SiH_3), where diffusion proceeds through motion of the physisorbed SiH_3 between Si-H sites. A relatively weak three-center bond structure is presumed, consistent with a small diffusion activation barrier. However, recent calculations of SiH_3/Si-H surface interactions[27] indicate that the three-center bond does not have a state sufficiently stable to account for observed diffusion processes. Another possible picture, also consistent with a relatively small diffusion activation energy, is that silyl radicals adsorb onto silicon sites and diffuse through Si-Si bond breaking and reforming, where bond breaking is facilitated by H insertion into the (weaker) stretched Si-Si bond, and Si-Si bond formation is accompanied by molecular hydrogen formation and release. Other elemental adsorption and diffusion steps could also be considered that are also consistent with the observed results.

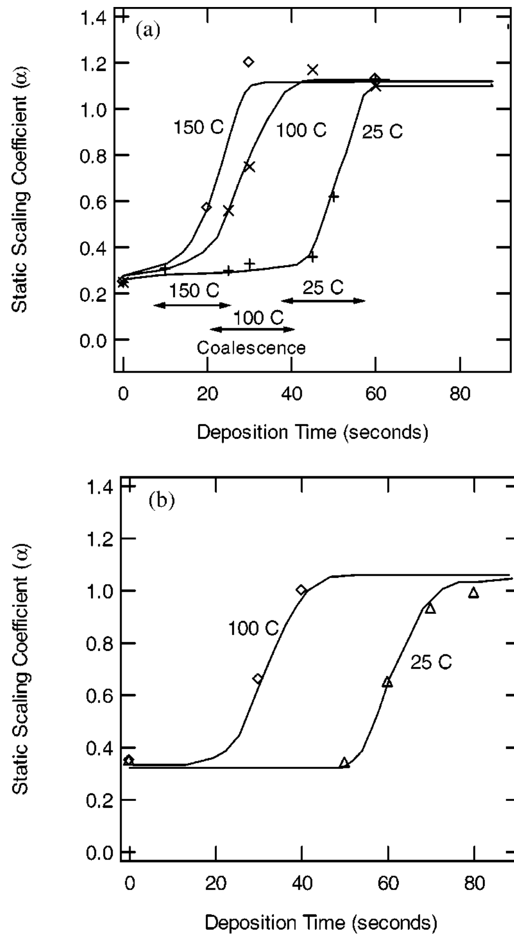

FIG. 7. Dependence of static scaling coefficient on deposition time and temperature for a-Si films deposited on (a) c-Si and (b) glass substrates. α increases with deposition time until it saturates at $\alpha=1$. The increase occurs more rapidly as temperature increases. Coalescence was determined by direct qualitative analysis of AFM images. A similar trend occurs for films grown on both c-Si and glass. The curves are guides for the eye.

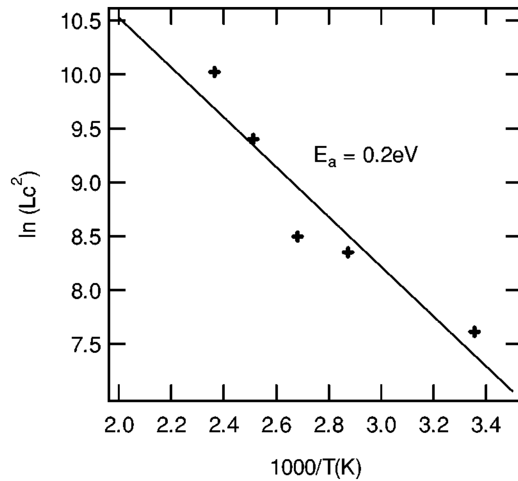

FIG. 8. Arrhenius plot of L_c^2 for samples deposited for 20 min. The linear slope indicates a thermally activated diffusion process with an activation energy of $E_a=0.2$ eV.

V. SUMMARY AND CONCLUSION

Fractal analyses, including dimensional and frequency methods, have been used to evaluate surface morphology of plasma deposited hydrogenated amorphous silicon surfaces formed under various deposition conditions. Using SiH_4/He mixtures, surface transport is dominated by surface diffusion, with a characteristic diffusion length that increases with surface temperature. Diffusion kinetics are consistent with a diffusion activation barrier of ~0.2 eV and with values estimated previously by other approaches. The coalescence of deposited film nuclei on the substrate surface is identified from the evolution of the static scaling coefficient. After initial nuclei coalescence, the surface topography of films formed from SiH_4/He mixtures is consistent with a self-similar geometry, independent of film thickness. Results in-

TABLE I. Summary of scaling coefficients, coalescence time and correlation length for various source gas, substrates, and substrate temperatures. The static scaling coefficient α is determined from dimensional analysis, and Fourier index is obtained from frequency analysis. N/A: Not Applicable.

Film (source gas)	Substrate	Substrate temp.	α	Fourier index	Coalescence time (s)	Correlation length (nm)	Self-similar?
None	c-Si		0.25		N/A	N/A	N
None	Corning 7059 glass		0.30		N/A	N/A	N
a-Si:H (SiH_4/He)	c-Si	25 °C	1.07	4.1	52	45	Y
		75 °C	1.04	4.7		65	Y
		100 °C	1.10	4.2	31	70	Y
		125 °C	1.00	4.3		110	Y
		150 °C	1.09	4.0	24	150	Y
a-Si:H (SiH_4/He)	Corning 7059 glass	25 °C	0.96	4.2	68	44	Y
		100 °C	1.00	4.5	36	62	Y
a-Si:H (SiH_4/Ar)	c-Si	25 °C	0.63	5.1		80	N
Evaporated Al	Quartz	25 °C	0.77	3.5		300	N

dicate that surface transport occurs by diffusion of adsorbed surface species, and the lateral correlation length increases from 45 to 150 nm as temperature increases from 25 to 150 °C. Argon dilution resulted in a more stochastic, rough surface, consistent with effects due to larger mass ion bombardment during deposition. The activation barrier of 0.2 eV obtained for silicon surfaces is smaller than 0.5 eV observed for diffusion on glassy metal surfaces, and is ascribed to effects of surface hydrogen in promoting diffusion of silicon adspecies. These results show that analysis of surface topography evolution can be used to obtain important surface kinetic parameters in the growth of silicon-based materials.

ACKNOWLEDGMENTS

This work was supported under NSF Grant Nos. 9624612 and 0072784. The authors also thank A. Flewitt and J. Robertson for helpful discussions and for sharing with us silicon samples and topological data.

[1] F. Family and T. Vicsek, J. Phys. A **18**, L75 (1985).
[2] A. L. Barabasi and H. E. Stanley, *Fractal Concepts in Surface Growth* (Cambridge University Press, Cambridge, 1995).
[3] W.M. Tong and R.S. Williams, Annu. Rev. Phys. Chem. **45**, 401 (1994).
[4] J. Robertson, J. Appl. Phys. **87**, 2608 (2000).
[5] J. Perrin, M. Shiratani, P. Kae-Nune, H. Videlot, J. Jolly, and J. Guillon, J. Vac. Sci. Technol. A **16**, 278 (1998).
[6] G. Ganguly and A. Matsuda, J. Non-Cryst. Solids **164-166**, 31 (1993).
[7] K. Maeda, A. Kuroe, and I. Umezu, Phys. Rev. B **51**, 10 635 (1995).
[8] A. Matsuda, Thin Solid Films **337**, 1 (1999).
[9] M.J. Kushner, J. Appl. Phys. **62**, 4763 (1987).
[10] K.K. Gleason, K.S. Wang, M.K. Chen, and J.A. Reimer, J. Appl. Phys. **61**, 2866 (1987).
[11] R. Robertson and A. Gallagher, J. Chem. Phys. **85**, 3623 (1986).
[12] B. Reinker, M. Moske, and K. Samwer, Phys. Rev. B **56**, 9887 (1997).
[13] M. Lutt, J.P. Schlomka, M. Tolan, J. Stettner, O.H. Seeck, and W. Press, Phys. Rev. B **56**, 4085 (1997).
[14] S.K. Sinha, E.B. Sirota, S. Garoff, and H.B. Stanley, Phys. Rev. B **38**, 2297 (1988).
[15] H. You, R.P. Chiarello, H.K. Kim, and K.G. Vandervoort, Phys. Rev. Lett. **70**, 2900 (1993).
[16] A.I. Oliva, J.L. Sacedon, E. Anguiano, M. Aguilar, J.A. Aznarez, and J.A. Mendez, Surf. Sci. **417**, L1139 (1998).
[17] C. Herring, J. Appl. Phys. **21**, 301 (1950).
[18] M. Kardar, G. Parisi, and Y.C. Zhang, Phys. Rev. Lett. **56**, 889 (1986).
[19] P. Meakin, *Fractals, Scaling and Growth Far From Equilibrium* (Cambridge University Press, Cambridge, 1998).
[20] M. Aguilar, E. Anguiano, and M. Pancorbo, J. Microsc. **172**, 233 (1993).
[21] S.J. Fang, S. Haplepete, W. Chen, C.R. Helms, and H. Edwards, J. Appl. Phys. **82**, 5891 (1997).
[22] W.U. Schmidt, R.C. Alkire, and A.A. Gewirth, J. Electrochem. Soc. **143**, 3122 (1996).
[23] D.M. Tanenbaum, A.L. Laracuente, and A. Gallagher, Phys. Rev. B **56**, 4243 (1997).
[24] M. Kondo, T. Ohe, K. Saito, T. Nishimiya, and A. Matsuda, J. Non-Cryst. Solids **227-230**, 890 (1998).
[25] H.-N. Yang, Y.-P. Zhao, G.-C. Wang, and T.-M. Lu, Phys. Rev. Lett. **76**, 3774 (1996).
[26] A.J. Flewitt, J. Robertson, W.I. Milne, J. Appl. Phys. **85**, 8032 (1999).
[27] A. Gupta, H. Yang, and G. N. Parsons, Surf. Sci (to be published).